Nanoelectronics and Its New Materials – A NEW ERA OF NANOSCIENCE

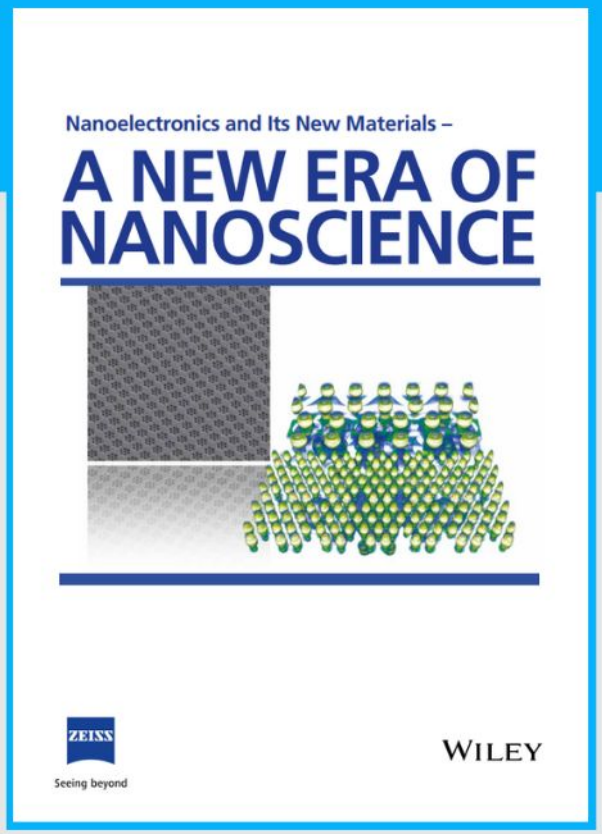

Discover the recent advances in electronics research and fundamental nanoscience.

Nanotechnology has become the driving force behind breakthroughs in engineering, materials science, physics, chemistry, and biological sciences. In this compendium, we delve into a wide range of novel applications that highlight recent advances in electronics research and fundamental nanoscience. From surface analysis and defect detection to tailored optical functionality and transparent nanowire electrodes, this eBook covers key topics that will revolutionize the future of electronics.

To get your hands on this valuable resource and unleash the power of nanotechnology, simply download the eBook now. Stay ahead of the curve and embrace the future of electronics with nanoscience as your guide.

ZEISS

Seeing beyond

WILEY

NANO · MICRO small
www.small-journal.com

Over One Million DNA and Protein Events Through Ultra-Stable Chemically-Tuned Solid-State Nanopores

Jugal Saharia, Yapa Mudiyanselage Nuwan Dhananjaya Yapa Bandara, Buddini Iroshika Karawdeniya, Jason Rodger Dwyer,* and Min Jun Kim**

Stability, long lifetime, resilience against clogging, low noise, and low cost are five critical cornerstones of solid-state nanopore technology. Here, a fabrication protocol is described wherein >1 million events are obtained from a single solid-state nanopore with both DNA and protein at the highest available lowpass filter (LPF, 100 kHz) of the Axopatch 200B–the highest event count mentioned in literature. Moreover, a total of ≈8.1 million events are reported in this work encompassing the two analyte classes. With the 100 kHz LPF, the temporally attenuated population is negligible while with the more ubiquitous 10 kHz, ≈91% of the events are attenuated. With DNA experiments, the pores are operational for hours (typically >7 h) while the average pore growth is merely ≈0.16 ± 0.1 nm h^{-1}. The current noise is exceptionally stable with traces typically showing <10 pA h^{-1} increase in noise. Furthermore, a real-time method to clean and revive pores clogged with analyte with the added benefit of minimal pore growth during cleaning (< 5% of the original diameter) is showcased. The enormity of the data collected herein presents a significant advancement to solid-state pore performance and will be useful for future ventures such as machine learning where large amounts of pristine data are a prerequisite.

1. Introduction

Nanopore sensing using solid-state nanopores (SSNs) is often positioned as a technology capable of accommodating the demands of the single-molecule research realm through high-throughput, label-free readout, and low-cost. However, unlike biological nanopores, SSNs have not advanced beyond the prototype level despite their promising start at the beginning of the millennium.[1] Five key challenges need to be met: size stability, long lifetime, resilience against clogging, low pore noise, and low fabrication cost. More critically, there should be minimal device-to-device variability in these key factors for SSNs to advance beyond the academic and prototype stage. While one could argue that the pores from nature tick all these boxes, SSNs open the door to, for example, more diverse geometries and devices and a wider range of material properties that are also amenable to chemical tuning for a host of different applications. While material, electronic, and chemical approaches have paved the way to lowering noise,[2–5] other challenges largely remained and were accepted, pending the development of any remedies, as a part of the science. The advent of controlled break-down (CBD)[6] and the real-time, solution-phase optimization for nm-level control of the fabrication process,[7] have transformed SSN technology and significantly lowered barriers to adoption. However, long operational lifetime, size stability, and resilience against clogging remained more elusive. Recently, we showed that a simple change to the electrolyte chemistry during fabrication by CBD, termed chemically-tuned CBD, or CT-CBD, leads to a longer pore lifetime (hours), greater stability (minimal change in open-pore conductance over time), and better resilience against analyte clogging (events >250 000).[8] These gains came via modification of only one of the CBD parameters—the solution chemistry. In conventional CBD, it is known that electric fields > 1 V nm^{-1} can lead to multiple pore formation.[9,10] In addition, while higher electric fields can support faster pore formation, the final pore properties (e.g., noise, lifetime, etc.) are less desirable than their low electric field counterparts. We were interested to know whether tuning the electric field magnitude during CT-CBD could also be used to further optimize the pore properties and by extension their performance.

J. Saharia, M. J. Kim
Department of Mechanical Engineering
Southern Methodist University
Dallas, TX 75275, USA
E-mail: mjkim@lyle.smu.edu
J. Saharia
Department of Mechanical Engineering
The University of Texas Permian Basin
Odessa, TX 79762, USA
Y. M. N. D. Y. Bandara
Research School of Chemistry
The Australian National University
Canberra, ACT 2601, Australia
E-mail: nuwan.bandara@anu.edu.au
B. I. Karawdeniya
Department of Electronic Materials Engineering
Research School of Physics
The Australian National University
Canberra, ACT 2601, Australia
J. R. Dwyer
Department of Chemistry
University of Rhode Island
140 Flagg Road, Kingston, RI 02881, USA
E-mail: jason_dwyer@uri.edu
The ORCID identification number(s) for the author(s) of this article can be found under https://doi.org/10.1002/smll.202300198.

DOI: 10.1002/smll.202300198

Longer reads, such as those of the human genome, require the pore to be open and stable for hours. While the focus of this study is not DNA sequencing, extending both the pore lifetime and stability is key for such efforts. We are confident that our achievement of over[1] million events from a single SSN will be a significant step forward in realizing the potential of SSNs for long DNA reads. One could potentially achieve a high event count with a larger pore. However, this comes at the expense of analyte confinement within the pore and signal-to-noise ratio (SNR). While higher bandwidths pave the way for the detection of fast translocations, the signal magnitude should be large enough to counter the higher open-pore noise at such operational bandwidths. Thus, the pore size should be carefully optimized to operate at a reasonably high bandwidth to minimize signal attenuation, maximize SNR, and achieve a high event count for statistical analysis. This serves as a more stringent (stress) test of the fabrication method benefits since (small) pores must be open and stable for hours to yield over[1] million events at the highest available LPF of the Axopatch 200B.

Resilience against pore clogging by the analyte is a key advantage of CT-CBD pores, most prominently manifested in the spontaneous recovery of the open-pore current after a sustained current occlusion too long to be ascribed to translocation. For more persistent clogs (with CT-CBD pores), recovery can be aided by setting the applied voltage bias to zero, by reversal of the applied bias polarity, or by the application of a ± 1.3 V pulse for few-milliseconds (a "zap").[8] For pernicious pore clogs, several voltage zaps may be required, and recovery of the open-pore current (and thus the recovery of well-conditioned pore function) is not guaranteed. In such instances, the pores are often discarded, thereby capping the number of events available for analysis. To avoid this finality, such clogged pores are often subjected to one or a variety of rinsing steps that generally preclude the real-time detection of pore unclogging. Certain analytes, such as highly charged biomolecules, are more likely to cause such troublesome pore clogs than others. We were interested in whether the basic premise of CT-CBD—the concerted use of chemical and electrical processing—could be used to develop a nanopore clog removal method with broad analyte scope and with real-time readout to detect pore rehabilitation more definitively.

In this study, we carefully scrutinized the CT-CBD pore fabrication process. It is known that the application of an electric field >1 V nm^{-1} leads to multiple pore formation while lower electric fields lead to higher fabrication times. In our previous study, we used electric fields of ≈0.7 V nm^{-1} for pore fabrication.[8] In this study, we observed that electric fields in the range of ≈0.45–0.7 V nm^{-1} can be used to fabricate pores in a reasonable time (an average of ≈12 min per pore). Four key features–lifetime, stability, resilience against clogging, and pore noise–were assessed initially with DNA across five LiCl concentrations (i.e., 4, 3, 2.5, 2, and 1 M) and later with a protein (human serum transferrin, hSTf). While it is customary to benchmark nanopore developments with DNA because of its well-defined chemical and physical properties, proteins provide a more stringent test as they can clog the pore through a multitude of different interactions and pose a greater risk of irreversible pore-clogging. Using hSTf, we easily reached our goal of over[1] million events from a single SSN. Overall, the manuscript contains ≈8.1 million events (with 100 kHz LPF)—the highest cumulative event count for a SSN study to the best of our knowledge. Our results thus show a reliable, and more importantly, a reproducible, methodology to achieve over 1 million events (from a single SSN) at the same time as having high pore lifetime, stability, and resilience against clogging which will be crucial for future advancement of SSN technology.

2. Results and Discussion

Despite high accuracy nanofabrication methods, variation in membrane thickness exists even for commercially available Si_xN_y membranes. This becomes a key factor during the CBD process for nanopore fabrication, where the same voltage applied through different membranes result in different magnitudes of leakage current (and break-down times). In our previous work, we applied an electric field of ≈0.7 V nm^{-1} till the initial break-down of the membrane.[8] In this work, electric fields between 0.45 and 0.7 V nm^{-1} were applied to one side of the membrane till the initial break-down or up to ≈10 min, whichever was the earliest. In case there was no break-downduring the first 10 min, the voltage polarity was reversed, and a lower electric field (between 0.35 and 0.55 V nm^{-1}) was applied. In most cases, the membrane dielectric break-down will occur in this step (indicated by a rapid surge in the current as seen in **Figure 1**a). In cases where no break-down occurred in the second step, the electric field polarity was switched again until a break-down event was observed. After the formation of the initial pore, short pulses (typically 1 s or 2 s) of lower voltage (electric field between ≈0.31 and ≈0.34 V nm^{-1}) were applied and *I–V* curves were obtained after each step (Figure 1b) to estimate pore diameter using a conductance model (Equation 1). These pulses were applied till a nanopore of the desired size was obtained. We used a total of 5 pores (≈10-12 nm)—one for each of the five different LiCl concentrations—while monitoring the previously mentioned four key parameters (i.e., stability, lifetime, resilience, and noise) with respect to DNA translocations. All five pores showed very high stability, long lifetime, high resilience against clogging, and stable noise profiles. From each of these five pores, we were able to independently collect >1 million events as shown in Figure 1c. More specifically, a total of ≈1.6 million (1 631 801), ≈1.4 million (1 406 415), ≈1.1 million (1 134 653), ≈1.9 million (1 888 728), and ≈1.1 million (1 090 149) events were collected using 4, 3, 2.5, 2, and 1 M LiCl respectively as seen in Figure 1c (cumulative count of ≈7.1 million (7 151 746) events). The event counts noted herein are the maximum we could obtain before the pore properties start to deteriorate due to repeated clogging by DNA. To the best of our knowledge, this is the first time where more than one million events with any analyte were acquired with a single SSN with SNR sufficient to operate at the highest available LPF of the Axopatch 200B. A brief comparison with existing literature is provided in Table S1 (Supporting Information). Figure 1d shows the current traces corresponding to all five electrolytes. To showcase the stability of the fabricated pores, we present time traces at the beginning (black), middle (maroon), and end (green) of the experiment. As seen, there is no visual change in the pore quality over time: the open-pore current stays stable over time for the traces

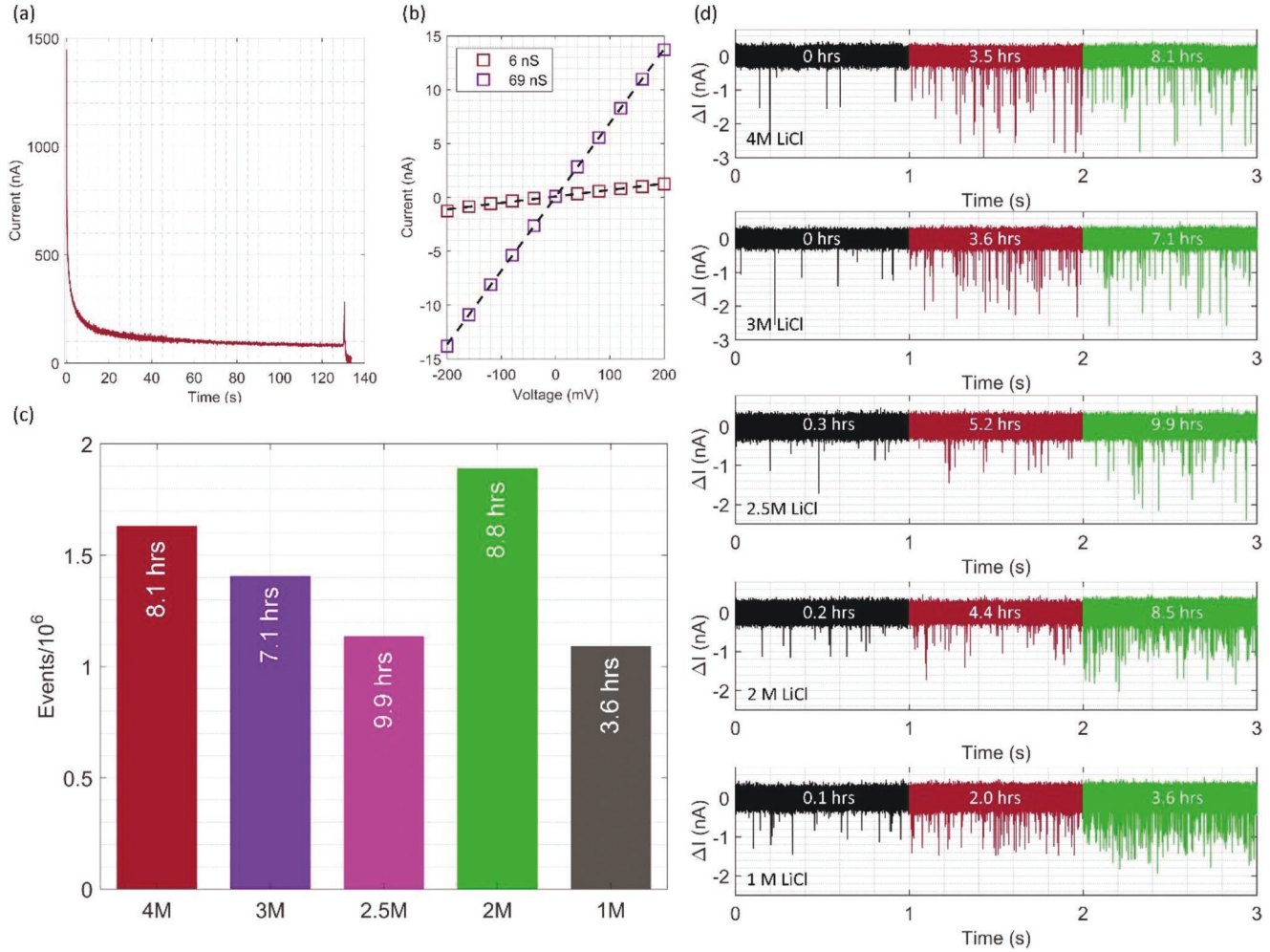

Figure 1. a) Current trace corresponding to controlled breakdown on a nominally ≈12 nm thick Si_xN_y with the application of an electric field of ≈0.53 V nm^{-1} for initial break-down. The sudden rise in current at ≈130 s indicates the formation of a pore. The LabVIEW script terminates the applied voltage once the current surges above the threshold set by $I_{cut\text{-}off}$. b) *I–V* curves corresponding to a nanopore formed immediately after the membrane break-down (≈6 nS) and after reaching the final desired size (≈69 nS) by application of low electric fields (≈0.32 V m^{-1}). This nanopore was used to obtain over one million DNA events in 2 M LiCl. c) Total number of DNA events collected (from five unique pores with one pore for each electrolyte concentration) with 4 M (1 631 801), 3 M (1 406 415), 2.5 M (1 134 653), 2 M (1 888 728) and 1 M (1 090 149) LiCl before irreversible clogging of the nanopores. The event counts noted herein are the maximum we could obtain before the pore properties start to deteriorate due to repeated clogging by DNA. The time each pore was open is indicated in white text. To achieve one million events, the time taken for each of the pores are as follows: ≈4.5 h (4 M), ≈5.9 h (3 M), ≈9.3 h (2.5 M), ≈5.9 h (2 M), and ≈3.5 h (1 M). d) One-second current traces corresponding to each of the LiCl concentrations at the beginning (black), middle (maroon), and end (green) of the translocation experiments with DNA. Corresponding experimental time is indicated in white text in each of the traces.

shown. Longer (300 s) are shown in Figure S-1A (Supporting Information) to further showcase the stability of the pores during DNA translocation. This is substantiated by the fact that the pore growth rate was a mere ≈0.16 ± 0.1 nm h^{-1} (on average) even after running the pores for several hours.

Molecular capture (event) rate is an important consideration in assays targeting high throughput. Significant changes in (cumulative) capture rate (C_R, events s^{-1}) have the potential to inform on changes to the nanopore shape or surface chemistry. **Figure2**a shows the evolution of cumulative capture rate with time. A constant voltage of 200 mV was applied continuously while recording the current until the occurrence of a significant clogging instance requiring user intervention. The C_R tended to be reduced noticeably in magnitude if the experiment was restarted after a 15–30 min pause (0 V applied across the pore) or if the contents were flushed with copious amounts of ultrapure water or unclogged by addition of NaOCl to the electrolyte (as described later)—a fresh aliquot of the analyte was needed to restart the translocations. Interestingly, we see that the C_R doesn't reach a steady-state value in any of the pores. This is especially clear with the 1 M LiCl run where it increases continuously over time (in a linear manner). The two higher concentrations (4 and, 3 M) seem to show an intermediate steady-state condition where event frequency seems to plateau briefly before increasing again. The enormity of the data collected herein showcases the perils of using arbitrary times for evaluation of C_R since, at least with 1 kb DNA and the salts used herein, there is a continuous increase in the C_R with time. Therefore, without

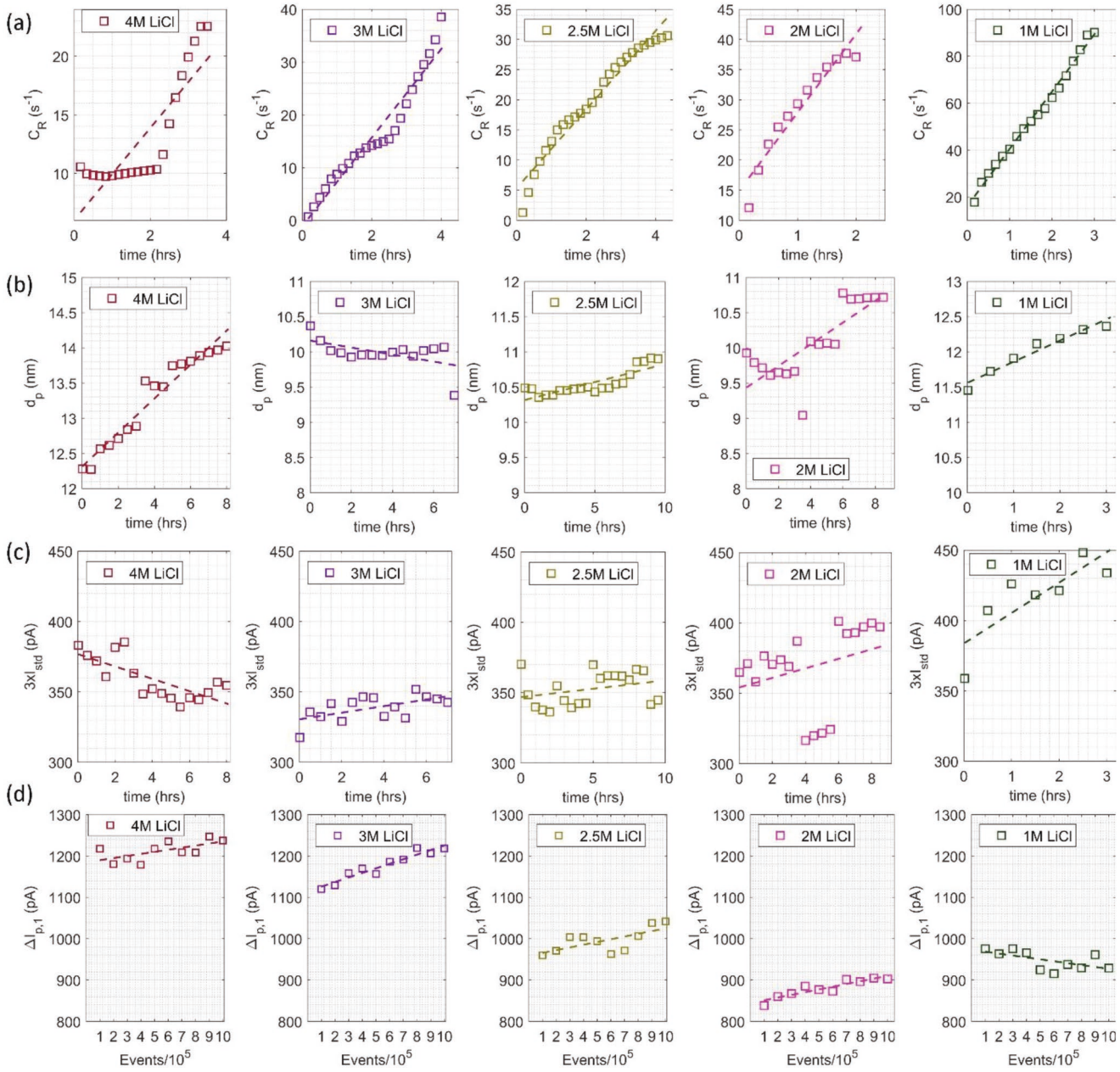

Figure 2. Evolution of a) cumulative capture rate (C_R) (shown until the first clogging instance), b) pore diameter (d_p), and c) three times the standard deviation of the pore-current ($3 \times I_{std}$) over time for the DNA translocations presented in Figure 1c. d) Evolution of the ΔI_P (see main text for the definition) corresponding to single-file DNA translocations ($\Delta I_{P,1}$) in each 100 k event segments (up to 1 million events) for the five electrolytes investigated in this study.

reaching a steady state value, the C_R values would change over time introducing random variability to the results. Considering the time scales used in this study ($\gtrsim$2 h for C_R data), waiting to reach a global steady state (for C_R) would be challenging. Although one could argue that the increase in the C_R over time could be due to pore growth over time—a common phenomenon with SSNs—Figure 2b shows that the pore growth, if any, is meager (≈0.3 nm h^{-1} at most). For example, visual inspection of the current trace corresponding to 1 M LiCl suggests very little pore growth while the capture rate for the pore increase with time. Thus, we could discredit a significant contribution from pore growth to the growing capture rate. Although the exact reasoning behind the fluctuating capture rate is not clear, it is evident that an alternative method for qualifying characteristics based on capture rate is necessary.[11]

Figure 2b presents the evolution of the pore diameter over time: no change in LiCl conductivity was observed for the duration of the experiments which discredits contributions from the change in electrolyte conductivity for the change in open-pore conductance and by extension the calculated pore diameter from Equation 1. We see the highest pore growth is associated with 4 M LiCl which is still <2 nm (≈14% of the

original diameter) over 8 h. A linear fit to the data reveals a measly growth of ≈0.24 nm h^{-1}. The growth of pore diameter in each of the LiCl concentrations was ≈0.24 nm h^{-1} (4 M LiCl), ≈0.05 nm h^{-1} (3 M LiCl), ≈0.05 nm h^{-1} (2.5 M LiCl), ≈0.15 nm h^{-1} (2 M LiCl), and ≈0.3 nm h^{-1} (1 M LiCl). While pore growth is an accepted part of SSNs, the growth rates from our fabrication protocol are minimal and would be crucial for the increased use of SSNs for lengthy sensing applications. While the pore grows at ≪ 1 nm h^{-1} rate, the pore noise (quantified using the three times the standard deviation of a Gaussian fit made to a current distribution from a 120 s-long trace, $3 \times I_{std}$, see Section S2, Supporting Information for more details) changes at ≈4.4 pA h^{-1} (4 M LiCl), ≈2.3 pA h^{-1} (3 M LiCl), ≈1.1 pA h^{-1} (2.5 M LiCl), ≈3.4 pA h^{-1} (2 M LiCl), and ≈21.6 pA h^{-1} (1 M LiCl) as seen in Figure 2c. The stability of the pores enumerated through the pore growth and $3 \times I_{std}$ values is also supported by the current traces shown in Figure 1d (and Figure S-1A, Supporting Information) where there is no visual change in the pore quality. Interestingly, we see a drop in the change in $3 \times I_{\text{std}}$ from 4 M LiCl to 2.5 M and thereafter increase with decreasing LiCl concentration. Moreover, the lowest concentration showed the highest $3 \times I_{\text{std}}$. At lower electrolyte concentrations, we observe a higher probability for reversible clogging which could lead to the observed $3 \times I_{\text{std}}$ trends. These growth statistics (both pore diameter and $3 \times I_{\text{std}}$) indicate, shorter experiments will see negligible changes to initial pore properties. We note that for the experiment with 1 M LiCl, the nanopore experienced notable reversible clogging towards the end of its lifetime unlike the pores used for the other concentrations where reversible clogging was minimal (Figure S-3A, Supporting Information). This can possibly be attributed to the extremely high C_R of DNA in 1 M LiCl compared to the other concentrations (Figure 2a). It should be noted that these occlusions are reversible–the pore can be revived by a zap potential, zero bias, or reversing the bias. We see electronically removable occlusions as an advantage since the operational software can be programmed to detect and remove a clog without user interference to indulge in a more thorough pore cleaning.

Next, we looked at the change in current (ΔI) characteristics originating from DNA translocations for all five LiCl concentrations (as a function of operational time). This was to see if there was any change in the ΔI characteristics with time or not. Since we have conducted experiments over ≈7 h in most cases and the availability of >1 million events meant, we could look at the ΔI characteristics for each set of 100 000 (100 k) events. The histograms were fitted with a Gaussian–Lorentzian Model and the peak ΔI (ΔI_P) corresponding to single file translocations ($\Delta I_{P,1}$) were plotted for every 100 k events as seen in Figure 2d (see associated discussion in Section S4, Supporting Information). The $\Delta I_{P,1}$ shows a linear relationship with time as seen in Figure 2d for all five LiCl concentrations. The rate of change was ≈5.0 pA h^{-1} (4 M LiCl), 11.1 pA h^{-1} (3 M LiCl), 6.6 pA h^{-1} (2.5 M LiCl), 6.6 pA h^{-1} (2 M LiCl), and ≈–4.6 pA h^{-1} (1 M LiCl). Since most nanopore experiments are designed to collect <10 000 events, the change in $\Delta I_{P,1}$ becomes less apparent. However, for DNA translocations using 4 M LiCl (run for ≈8 h), we see a shift of ≈40 pA for $\Delta I_{P,1}$. Although these values are negligible, it is interesting to note that $\Delta I_{P,1}$ grows with time. Considering that the pore diameter also grows at a slower rate over time, it could not explain the growth of $\Delta I_{P,1}$ since an increase in pore diameter should not typically lead to an increase in $\Delta I_{P,1}$. Another interesting observation is the decrease of $\Delta I_{P,1}$ with time in 1 M LiCl. While the exact reasoning behind these changes is not clear, it is evident that the $\Delta I_{P,1}$ corresponding to DNA translocations changes with time and histograms of ΔI should be constructed diligently to avoid averaging of temporal changes. Interestingly, we see that the ΔI distribution becomes narrower with decreasing LiCl concentration while promoting single-file translocations (Figure S4, Supporting Information). This is expected since with decreasing LiCl concentration, the opposing electroosmotic flow increases which lead to more single-file translocations.[12] We note that all experiments were run at room temperature. However, we did not use a temperature controller to maintain a near-perfect isothermal condition for the experiments. Thus, solution temperature could increase (although ever so slightly) over time during such lengthy experiments which could also contribute to the observed pore diameter and $\Delta I_{P,1}$ growth trend with time. $\Delta I_{P,1}$ with voltage showed a linear relationship suggesting a diffusion limited translocation mechanism (data not shown). Information about translocation time can also be found in Section S4 (Supporting Information).

Although we have elaborated a protocol to produce pores resistant to clogging, in reality, all pores clog at some point. The usual practice then is to attempt a revival of the pore through methods mentioned previously in the paper. However, often pores clog irreversibly that renders them futile for further use. Thus, a real-time cleaning method that can be monitored through the amplifier (Axopatch 200B in this case) would greatly improve the ability of the user to revive the pore since there is a visual indication as to when the pore becomes free of its previously clogged stage. Here, we show that the addition of NaOCl to a clogged pore under an electric-field could revive it while providing real-time data on the cleaning process. For this, we used a pore that was run for ≈4 h and produced >750 000 events (**Figure3**a). Afterward, the pore started partially clogging repeatedly and efforts to revive it using electrical methods proved futile as seen in Figure 3b. In this case, the DNA clogs the pore from its open-pore values of ≈9.3 to ≈8.5 nA in a single step. Such single-step clogging is commonly seen with DNA. To revive the pore, as seen in Figure 3c, we added 100 µL of NaOCl (9:2 (v:v) LiCl: NaOCl) to one chamber around the 15 s mark while holding the potential at + 200 mV. The absence of data at ≈15 s and ≈25 s is due to the opening of the Faraday cage to add NaOCl. We can see that more stochastic events start to appear (instead of closely spaced current perturbations that is observed just before the opening of the Faraday cage). However, the baseline looks unstable as evident through the trace segment between ≈16–24 s. Afterward, the Faraday cage was opened again to add 100 µL of NaOCl to the other chamber (9:2 (v:v) LiCl: NaOCl). We can see that the open-pore current further increased upon the addition of NaOCl to the other chamber and then reaches a steady state. Afterward, the solution was exchanged with fresh LiCl, and the pore was run after adding DNA to the *cis* side (Figure 3d). As seen, there is a time lag for the onset of events (as expected, since molecules have to diffuse to the capture zone before undergoing drift-dominated

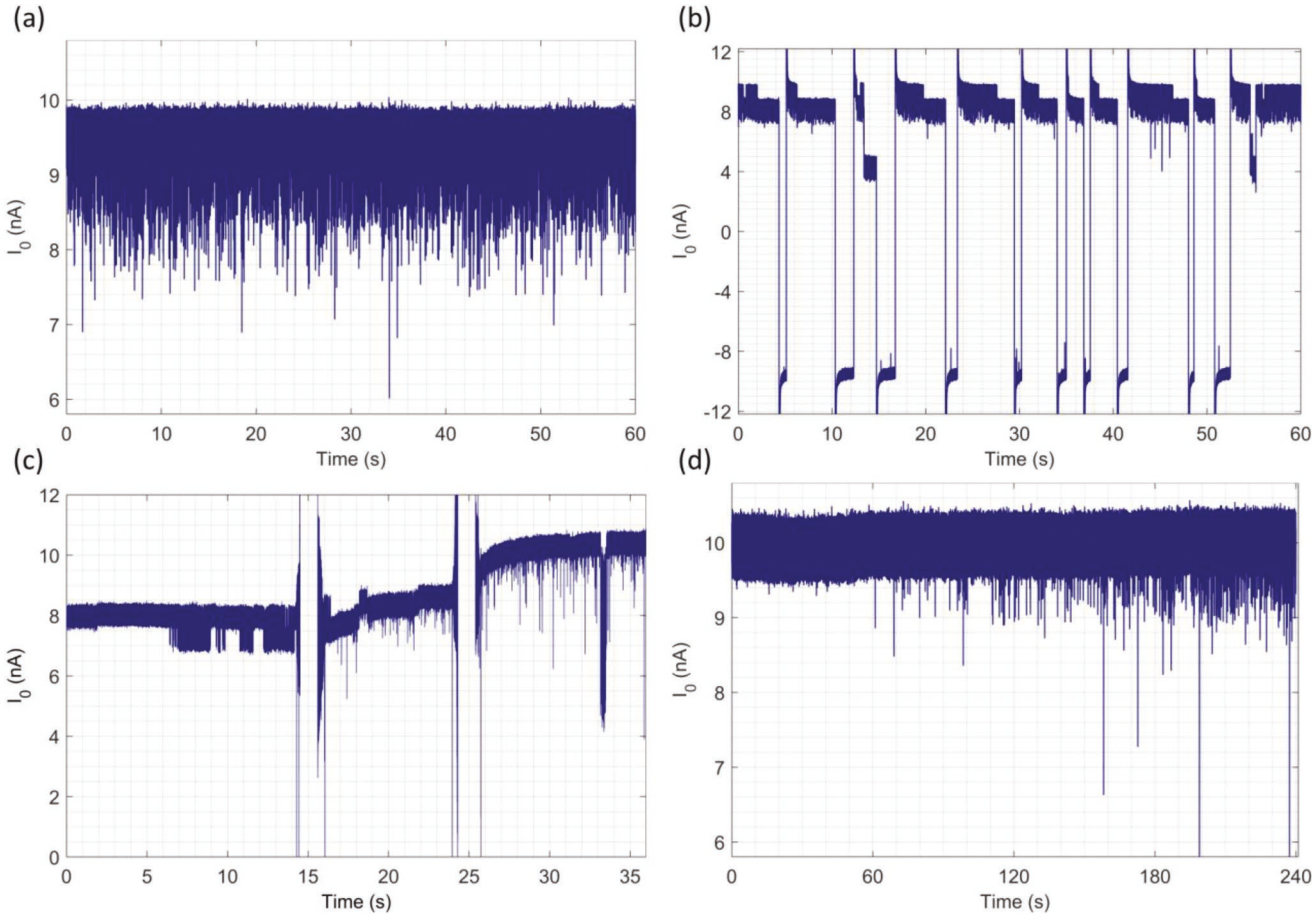

Figure 3. a) 60 s trace corresponding to DNA translocating through a ≈10 nm pore under +200 mV of applied voltage (2 M LiCl, pH≈7.5). b) After ≈4 h of continuous running, the pore started to clog repeatedly and attempts to revive the pore with a zap potential were short-lived as the pore would go back to clogged state shortly afterward. c) Addition of bleach (i.e., NaOCl) to revive the pore (see main text) and d) DNA translocations through the revived pore which was then run for ≈4.7 h to collect 1 126 747 events (note: the pore did not clog afterward).

transport), and the rate increases afterward. The open-pore current before and after the cleaning was ≈9.28 nA and ≈9.95 nA, respectively which correlate to a mere ≈4.4% growth in pore diameter. Thus, the addition of NaOCl does not increase the pore diameter considerably and helps to revive the pore for future experiments. From the relative current drop histograms of DNA translocation events before and after this cleaning process (Figure S5, Supporting Information), we also confirmed that cleaning of the pore by this method did not alter its sensing results. We believe that these findings would be extremely useful for commercial devices where upon clogging with the analyte, the pore could be revived by controlling the addition of bleach and flushing with fresh electrolyte. The same cleaning method was attempted with a pore clogged with hSTf in a separate experiment (Figure S6, Supporting Information) where, similar to Figure 3, a negligible change in the open-pore current was seen. Another advantage of NaOCl is its ability to remove biological material from the nanopore system through oxidation (or other chemical means that lead to the degradation of the structure). Thus, the proposed NaOCl real-time cleaning can also be envisioned as a method to clean a pore between two experiments.

Compared to homogeneously charged DNA, protein transport through a nanopore is more challenging due to its complex structure and heterogeneous charge distribution. Non-specific adsorption of proteins[13–15] is a well-reported phenomenon and steps such as functionalization and antifouling[16–18] are undertaken to minimize such adsorption. However, surface functionalization requires an additional post-fabrication modification step and can potentially change nanopore properties. After successfully obtaining over one million DNA translocation events from a single nanopore, we sought to obtain similar results for protein experiments. Instead of functionalization, the CT-CBD method relies on the chemical tuning of the nanopore surface during the fabrication step, and therefore, CT-CBD nanopores with longer sensing time and minimal protein adsorption will be of great significance. We chose the holo form of hSTf for our experiment because of its well-documented translocation characteristics.[19–23] With the modified fabrication protocol, we were able to obtain over one million (1 030 404) events using a ≈16 nm pore and those events were obtained with 100 kHz LPF (**Figure 4**a). While a higher count could be recorded with the more ubiquitous 10 kHz LPF due to lower noise, the temporal attenuation threshold (TAT)

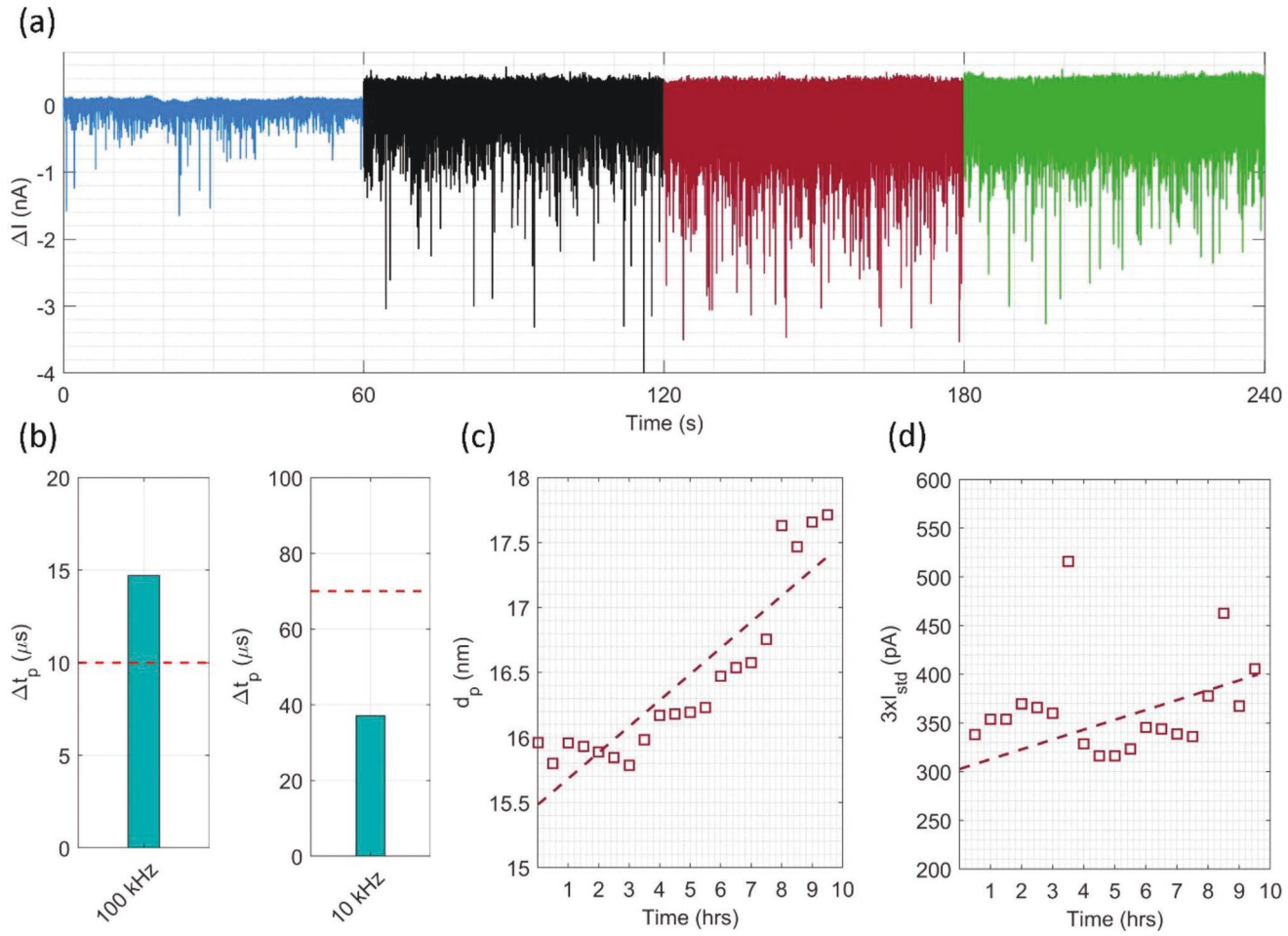

Figure 4. a) 60 s current trace at 10 kHz LPF (blue) and those corresponding to beginning (black), middle (maroon) and the end (green) of the translocation experiments with hSTf at 100 kHz LPF. b) The Δt_P (i.e., peak translocation time) corresponding to 100 and 10 kHz LPF settings. The dashed lines in each case indicate the temporal attenuation threshold corresponding to each LPF setting. The evolution of c) pore diameter and d) three times the standard deviation of the pore-current ($3 \times I_{std}$) over time for the hSTf translocations

of the two filter settings and the translocation speed of hSTf dictate that more useful information could be gathered with 100 kHz LPF. That is, the TAT for 10 and 100 kHz filters are ≈70 and ≈10 µs respectively (note that in the resistive feedback mode, the bandwidth only reaches up to 70 kHz).[24] The histogram corresponding to translocation time was fitted with $f(\tau) = \frac{l}{\sqrt{4\pi D\tau^3}} \exp\left(-\frac{(l-\upsilon\tau)^2}{4D\tau}\right)$ where D, l, and υ the diffusion coefficient, effective sensing length and drift velocity of hSTf. The peak of this fit (Δt_P) for both the filter settings is shown in Figure 4b. We see that ≈91% of the population is temporally attenuated with the 10 kHz LPF while that number is negligible with the 100 kHz filter. Thus, not only breaching the 1 million barrier, but also gathering temporally non-attenuated events are crucial. To this extent, we believe, this is the highest event count reported for a protein at 100 kHz LPF through a single SSN. Similar to DNA experiments, we monitored the evolution of event frequency, pore diameter, and $3 \times I_{std}$ over time for this pore where we saw an increase of ≈0.2 nm h^{-1} and ≈10.1 pA h^{-1} respectively (Figure 4c,d)—comparable to those observed with DNA translocations.

3. Conclusion

In this work, we have presented a fabrication protocol to produce pores with ultra-stability, lifetime, resilience against clogging, and throughput. Moreover, the pores were conducive to running with both DNA and hSTf (protein) with the highest available LPF of the ubiquitous amplifier of choice, the Axopatch 200B. The pores typically stayed open for >7 h (unless one million events were achieved before that) and produced >1 million DNA events each for five different LiCl concentrations. With proteins, only a single electrolyte concentration was carried out for the demonstration purpose of reaching >1 million events. These are the highest recorded event counts from a single SSN with 100 kHz LPF. Overall, a total of ≈8.1 million events were recorded (including both 10 and 100 kHz recordings for DNA and hSTf), which to the best of our knowledge is the largest collection presented in a single SSN study. A negligible number of events was attenuated for hSTf with the 100 kHz LPF setting. However, the attenuation percentage increased significantly to ≈91% with the more ubiquitous LPF of choice, 10 kHz. While one could also attempt to breach the 1 million event barrier

with a larger pore by loading a high amount of protein or running the experiment for a long time with a lower protein concentration, we chose the more challenging path by setting LPF at 100 kHz: small enough pores must be used to maximize SNR for event detection. However, even with proteins, we see that the pores stay open for hours. The noise (estimated as the standard deviation of the open-pore current), does not change appreciably over time. The average pore growth was a mere ≈0.16 ± 0.1 nm h^{-1} which is exceptional considering the time scale at which the experiments were conducted. This stability was also evident through the raw-current traces where there was no visual change in the noise at the beginning, middle, and end of the pore lifetime. To tackle the intractable clogging issue, we also demonstrated a real-time cleaning method with bleach as an additive to the electrolyte in an electric field where the user could "see" the CT-CBD pore being revived in real-time. This pore size is increased by a mere <5% of the starting value (0.15 nm h^{-1} on average) by this method and given its effectiveness in cleaning and reviving occluded pores, it could have applications in the commercial space.

While SiN_x nanopores fabricated through CBD are net negatively charged at the operational pH (i.e., ≈7.5), those fabricated from the CT-CBD are net-neutral. Thus, electroosmosis—fluidic movement inextricably linked to the counter ion layer proximal to the surface head groups—is meager (if not absent) in SiN_x pores fabricated through CT-CBD (unlike CBD). At pH ≈7.5, DNA is net negatively charged. Thus, for translocations to be feasible from the cis to the trans direction, a positive voltage bias needs to be applied. Since the pore surface of those fabricated from CBD is net negatively charged, the motion of the counter-ion layer and by extension electroosmosis would be in the opposing direction to the DNA translocation (i.e., trans to cis). On the contrary, due to the absence of surface charge of pores fabricated through the CT-CBD process, there is no (or very minimal at best) electroosmosis opposing the translocation of DNA through the nanopore. This would increase the C_R with CT-CBD pores compared to CBD pores. The absence of a charged surface (in the case of CT-CBD) could also be contributing to the minimal analyte occlusions seen with CT-CBD fabricated pores which leads to high lifetime and by extension the ability to capture over 1 million events as noted in this work. Furthermore, it is important to note that the surface charge (whether it is of the analyte or the nanopore surface) has implications on dwell time and signal magnitude as well. Since CBD pores do not stay open for a long period like the CT-CBD fabricated pores, it is not possible to make a conclusive comparison of the two methods (over hours of operation). However, compared to CBD pores, CT-CBD fabricated pores deliver superior outcomes which could be tightly linked to the differences in surface chemistries of pores from the two fabrication methods.

Thus, we see, that the advancements we have documented could propel the SSN technology to the much-anticipated commercial space.

4. Experimental Section

Nanopore Fabrication: Nominally ≈12 nm thick silicon nitride (Si_xN_y) membranes (NBPX5001Z-HR, Norcada Inc.) were mounted between custom-made Teflon half cells. The two electrolyte reservoirs (i.e., *cis* and *trans*) were filled with 2:9 (in volume) NaOCl (425 044, Sigma–Aldrich): 1 M KCl (P9333, Sigma–Aldrich). Voltage bias was applied as outlined in the Results and Discussion Section until a sudden surge of current was seen. Afterward, the solution was exchanged multiple times with DI water followed by LiCl (213 233, Sigma–Aldrich) used for translocation experiments for pore nanopore size estimation.

Nanopore Size Estimation: After the initial break-down, a current–voltage (*I–V*) curve was obtained and the diameter of the fabricated nanopores was estimated using the slope of the curve (i.e., conductance) with the aid of a conductance model:

$$G = K\left(\frac{1}{\frac{\pi r_0^2}{L} + \frac{\mu|\sigma|}{K}\cdot\frac{2\pi r_0}{L}} + \frac{2}{\alpha\cdot 2r_0 + \beta\cdot\frac{\mu|\sigma|}{K}}\right)^{-1} = \left(\frac{1}{G_{\text{bulk}} + G_{\text{surface}}} + \frac{1}{G_{\text{access}}}\right)^{-1} \quad (1)$$

where G, K, L, r_o, σ, μ, α, and β are the ionic conductance, electrolyte conductivity, membrane thickness, nanopore radius, nanopore surface charge density, surface counterion mobility, and model-dependent parameters (both set to 2) respectively.[25,26] The contribution of σ to G at the operational pH (i.e., ~7.5) is negligible and can be disregarded. The framework for the evaluation of σ can be found in our previous work.[8] Afterward, if needed, the pore was enlarged by applying electric fields as described in the Results and Discussion Section.

Electrolyte Preparation: All experiments were carried out with LiCl as the principal electrolyte salt. All electrolytes were prepared by dissolving the as-supplied LiCl in ultra-pure water (>18 MΩ cm) followed by the addition of Tris buffer (J61036, Fisher Scientific) to a final concentration of 10 mM. Solutions were then filtered using 0.22 µm filters (S2GPT05RE, Fisher Scientific). The pH was adjusted by adding concentrated drops of HCl (H1758, Sigma–Aldrich) or KOH (306 568, Sigma–Aldrich) and measured using an Orion Star pH meter.

Biomolecule Preparation: Double-stranded DNA (10 787 018, Fisher Scientific) was added to the *cis* chamber to a final concentration of 25 µg mL^{-1} (in 4, 3, and 2.5 M LiCl) and 50 µg mL^{-1} (in 2 and 1 M LiCl). The DNA ladder chosen for this study consisted of DNA fragments in the range of 100–15 000 bp. More specifically, the DNA length and its composition (ng per 0.5 µg) was as follows: 100 bp (40), 200 bp (30), 300 bp (30), 400 bp (30), 500 bp (30), 650 bp (30), 850 bp (30), 1000 bp (30), 1500 bp (70), 2000 bp (20), 3000 bp (20), 4000 bp (20), 5000 bp (20), 6000 bp (20), 7000 bp (20), 8000 bp (20), 10 000 bp (20), 15 000 bp (20). Stock solutions of human serum transferrin (hSTf, T0665, Sigma–Aldrich) were prepared by dissolving the as-supplied powder in ultra-pure water and stored at 4 °C until use (used within 7 days). hSTf was added to the *cis* chamber to a final concentration of 250 nM.

Electrical Measurements: All electrical measurements were done using an Axopatch 200B (Molecular Devices) connected to a Digidata 1550B (Molecular Devices) digitizer. The lowpass filter (LPF) was either set to 10 kHz (protein) or 100 kHz (DNA and protein). Data were acquired at a rate of 500 kHz. All extractions were done using the EventPro platform (version 3.0)[27] and analyzed using custom MATLAB and Mathematica scripts. While an event is defined as a resistive perturbation that is deeper than a user-defined threshold (600 pA in this study), it constitute both bumps and true translocations. In this study, while the total number of events is reported, translocations were defined as temporally non-attenuated events. Since the Axopatch 200B in resistive feedback mode reaches a bandwidth of 70 kHz, the temporal attenuation threshold would be 10 µs. For all the electrolyte concentrations, events faster than 10 µs were <0.5%—a negligible amount. These events are shown in Figure S1B (Supporting Information) and more details can be found in Section S4 (Supporting Information) as well.

Supporting Information

Supporting Information is available from the Wiley Online Library or from the author.

Acknowledgements

This work was financially supported by the National Science Foundation (CBET #2022398 and #2022374) and the National Institute of Health (R21CA240220). Y.M.N.D.Y.B. and B.I.K. would also like to acknowledge the Australian National University Grand Challenge ''Our Health in Our Hands''. The authors would also like to thank Dr. Madhav Ghimire for his inputs. All authors would like to thank their respective institutions for the software suites provided for the analyses presented in this study.

Conflict of Interest

The authors declare no conflict of interest.

Data Availability Statement

The data that support the findings of this study are available from the corresponding author upon reasonable request.

Keywords

high-lifetime, low-noise, million events, nanopores, ultra-stable

Received: January 8, 2023
Revised: March 7, 2023
Published online: April 7, 2023

[1] J. Li, D. Stein, C. McMullan, D. Branton, M. J. Aziz, J. A. Golovchenko, *Nature* **2001**, *412*, 166.
[2] J. K. Rosenstein, M. Wanunu, C. A. Merchant, M. Drndic, K. L. Shepard, *Nat. Methods* **2012**, *9*, 487.
[3] I. Yanagi, K. Takeda-i, *Nanotechnology* **2021**, *32*, 415301.
[4] V. Tabard-Cossa, D. Trivedi, M. Wiggin, N. N. Jetha, A. Marziali, *Nanotechnology* **2007**, *18*, 305505.
[5] Z. Zhu, X. Duan, Q. Li, R. Wu, Y. Wang, B. Li, *J. Am. Chem. Soc.* **2020**, *142*, 4481.
[6] H. Kwok, K. Briggs, V. Tabard-Cossa, *PLoS One* **2014**, *9*, e92880.
[7] M. Waugh, K. Briggs, D. Gunn, M. Gibeault, S. King, Q. Ingram, A. M. Jimenez, S. Berryman, D. Lomovtsev, L. Andrzejewski, *Nat. Protoc.* **2020**, *15*, 122.
[8] D. Y. Bandara, M. N. Y. , J. Saharia, B. I. Karawdeniya, J. T. Hagan, J. R. Dwyer, M. J. Kim, *Nanotechnology* **2020**, *31*, 335707.
[9] Y. Wang, C. Ying, W. Zhou, L. de Vreede, Z. Liu, J. Tian, *Sci. Rep.* **2018**, *8*, 1234.
[10] C. Ying, J. Houghtaling, O. M. Eggenberger, A. Guha, P. Nirmalraj, S. Awasthi, J. Tian, M. Mayer, *ACS Nano* **2018**, *12*, 11458.
[11] M. Charron, K. Briggs, S. King, M. Waugh, V. Tabard-Cossa, *Anal. Chem.* **2019**, *91*, 12228.
[12] N. Ermann, N. Hanikel, V. Wang, K. Chen, N. E. Weckman, U. F. Keyser, *J. Chem. Phys.* **2018**, *149*, 163311.
[13] H. Tian, W. Xie, S. He, D. Zhou, S. Fang, L. Liang, D. Wang, *RSC Adv.* **2019**, *9*, 15431.
[14] E. C. Yusko, J. M. Johnson, S. Majd, P. Prangkio, R. C. Rollings, J. Li, J. Yang, M. Mayer, *Nat. Nanotechnol.* **2011**, *6*, 253.
[15] S. Balme, P. E. Coulon, M. Lepoitevin, B. Charlot, N. Yandrapalli, C. Favard, D. Muriaux, M. Bechelany, J.-M. Janot, *Langmuir* **2016**, *32*, 8916.
[16] N. Giamblanco, D. Coglitore, J.-M. Janot, P. E. Coulon, B. Charlot, S. Balme, *Sens. Actuators, B* **2018**, *260*, 736.
[17] R. Hu, J. Diao, J. Li, Z. Tang, X. Li, J. Leitz, J. Long, J. Liu, D. Yu, Q. Zhao, *Sci. Rep.* **2016**, *6*, 1.
[18] X. Li, R. Hu, J. Li, X. Tong, J. Diao, D. Yu, Q. Zhao, *Appl. Phys. Lett.* **2016**, *109*, 143105.
[19] Y. N. D. Bandara, N. Farajpour, K. J. Freedman, *J. Am. Chem. Soc.* **2022**, *144*, 3063.
[20] J. Saharia, Y. N. D. Bandara, M. J. Kim, *Electrophoresis* **2022**, *43*, 785.
[21] J. Saharia, Y. N. D. Bandara, G. Goyal, J. S. Lee, B. I. Karawdeniya, M. J. Kim, *ACS Nano* **2019**, *13*, 4246.
[22] J. Saharia, Y. N. D. Bandara, B. I. Karawdeniya, C. Hammond, G. Alexandrakis, M. J. Kim, *RSC Adv.* **2021**, *11*, 24398.
[23] B. YMNDY, K. Freedman, *ACS Nano* **2022**, *16*, 14111.
[24] D. R. Garalde, O'C. R. Donnell, R. D. Maitra, D. M. Wiberg, G. Wang, W. B. Dunbar, *IEEE Trans Control Syst Technol* **2012**, *21*, 2038.
[25] F. Detcheverry, L. Bocquet, *Phys. Rev. Lett.* **2012**, *109*, 024501.
[26] Y. N. D. Bandara, B. I. Karawdeniya, J. R. Dwyer, *ACS Omega* **2019**, *4*, 226.
[27] Y. N. D. Bandara, J. Saharia, B. I. Karawdeniya, P. Kluth, M. J. Kim, *Anal. Chem.* **2021**, *93*, 11710.